JACS
JOURNAL OF THE AMERICAN CHEMICAL SOCIETY

Article

pubs.acs.org/JACS

Smart Near-Infrared Fluorescence Probes with Donor−Acceptor Structure for in Vivo Detection of β-Amyloid Deposits

Mengchao Cui,[†,‡] Masahiro Ono,[*,†] Hiroyuki Watanabe,[†] Hiroyuki Kimura,[†] Boli Liu,[‡] and Hideo Saji[†]

[†]Department of Patho-Functional Bioanalysis, Graduate School of Pharmaceutical Sciences, Kyoto University, 46-29 Yoshida Shimoadachi-cho, Sakyo-ku, Kyoto 606-8501, Japan

[‡]Key Laboratory of Radiopharmaceuticals, Ministry of Education, College of Chemistry, Beijing Normal University, Beijing 100875, P. R. China

Supporting Information

ABSTRACT: The deposition of β-amyloid (Aβ) plaques in the parenchymal and cortical brain is accepted as the main pathological hallmark of Alzheimer's disease (AD); however, early detection of AD still presents a challenge. With the assistance of molecular imaging techniques, imaging agents specifically targeting Aβ plaques in the brain may lead to the early diagnosis of AD. Herein, we report the design, synthesis, and evaluation of a series of smart near-infrared fluorescence (NIRF) imaging probes with donor−acceptor architecture bridged by a conjugated π-electron chain for Aβ plaques. The chemical structure of these NIRF probes is completely different from Congo Red and Thioflavin-T. Probes with a longer conjugated π system (carbon−carbon double bond) displayed maximum emission in PBS (>650 nm), which falls in the best range for NIRF probes. These probes were proved to have affinity to Aβ plaques in fluorescent staining of brain sections from an AD patient and double transgenic mice, as well as in an in vitro binding assay using $Aβ_{1-42}$ aggregates. One probe with high affinity (K_i = 37 nM, K_d = 27 nM) was selected for in vivo imaging. It can penetrate the blood−brain barrier of nude mice efficiently and is quickly washed out of the normal brain. Moreover, after intravenous injection of this probe, 22-month-old APPswe/PSEN1 mice exhibited a higher relative signal than control mice over the same period of time, and ex vivo fluorescent observations confirmed the existence of Aβ plaques. In summary, this probe meets most of the requirements for a NIRF contrast agent for the detection of Aβ plaques both in vitro and in vivo.

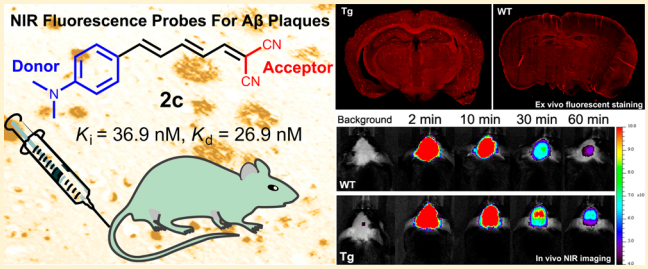

INTRODUCTION

Alzheimer's disease (AD), a neurodegenerative disease, is the most common cause of dementia among older people. Currently, there are no available treatments that stop or reverse the progression of the disease, and only a few medicines can alleviate the symptoms. Moreover, the clinical diagnosis of AD is primarily from the patient history, collateral history from relatives, and neurological and neuropsychological observations, so doctors can only make a diagnosis of possible or probable AD. A confirmatory diagnosis can only be made after autopsy by examining brain tissues to confirm the existence of β-amyloid (Aβ) plaques and neurofibrillary tangles (NFTs).[1,2] According to the amyloid cascade hypothesis, Aβ deposition in the brain is thought to be the fundamental cause of AD and appears to be good diagnostic and predictive biomarker for this disease. Detection of Aβ in vivo will be important for the early differential diagnosis of dementia, predicting the progression of AD, as well as monitoring the effectiveness of novel anti-Aβ drugs for AD.[3−6] Over the past decades, there have been numerous advances in the development of radiolabeled Aβ imaging probes for positron emission tomography (PET) and single photon emission computed tomography (SPECT) based on the structures of Congo Red (CR) and Thioflavin T (ThT).[7−10] To date, [^{11}C]PIB is the most extensively studied PET imaging probe for Aβ plaques in humans,[11−13] while [^{18}F]AV-45 is the first Aβ imaging probe approved by the FDA (Figure 1);[14−17] however, the major disadvantages of the classical nuclear imaging modalities include high cost, exposure to radioactivity, and a time-consuming data acquisition process.

Compared with nuclear imaging modalities, the optical imaging modality possesses many advantages, as it enables safe

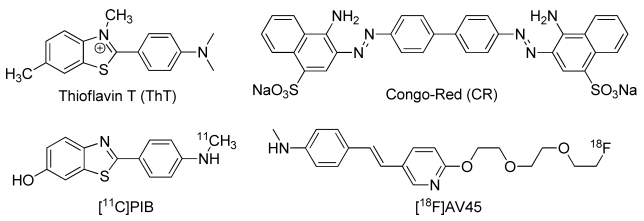

Figure 1. Chemical structures of the common Aβ-specific dyes, Congo Red and Thioflavin-T, and Aβ imaging probe [^{11}C]PIB and [^{18}F]AV-45.

Received: May 26, 2013
Published: February 20, 2014

   dx.doi.org/10.1021/ja4052922 | J. Am. Chem. Soc. 2014, 136, 3388−3394

detection without radiation exposure and real-time imaging without a time-consuming data acquisition process and requires readily available instruments at moderate cost without expensive equipment and a combination of highly skilled personnel.[18−21] However, the emission wavelength of the fluorescent probes developed for optical imaging is usually less than 550 nm, which will interfere with autofluorescence from biological matter in vivo and limit their in vivo usage. To obtain an acceptable penetration depth and high sensitivity, NIRF imaging has emerged as an attractive tool for optical imaging. A number of commercially available NIR fluorophores have been developed and employed for in vivo imaging, including Indocyanine Green dyes (ICG), Cyanine dyes (Cy), IRdye dyes, Alexa Fluor dyes, and SRfluor Dyes.[21] Due to the large molecular weight and intrinsic charge of these NIR fluorophores, they are usually used to label biologically active peptides for targets other than the brain. Thus, a small, compact NIR fluorophore (emission wavelength >650 nm) that could rapidly penetrate the intact blood−brain barrier (BBB) is required for the development of Aβ NIRF probes. To date, there have been few reports regarding the development of NIRF probes for the detection of Aβ plaques, and most of them are highly conjugated molecules based on the donor−acceptor or donor−acceptor−donor architecture bridged by a conjugated π-electron chain (Figure 2). In 2005, an oxazine

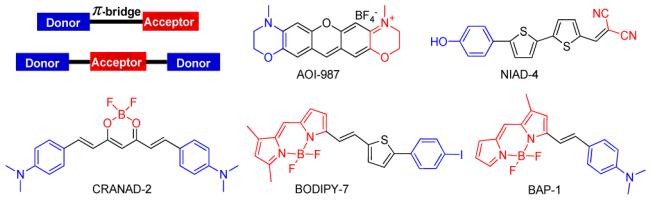

Figure 2. NIRF probes reported previously for the detection of Aβ plaques based on donor−acceptor and donor−acceptor−donor backbones.

derivative, AOI-987, was reported as an efficient NIRF probe for Aβ imaging;[22] however, AOI-987 displayed moderate affinity (K_d = 220 nM) to Aβ aggregates and is a charged molecule, which may reduce brain penetrability. Swager et al. reported a highly polarizable bithiophene derivative, NIAD-4, which displayed high affinity to Aβ aggregates (K_i = 10 nM).[23] In vivo imaging data from transgenic mice demonstrated that NIAD-4 could readily cross the BBB and label Aβ plaques specifically. However, the emission wavelength is only 603 nm, out of the NIR range. On the basis of the donor−acceptor−donor architecture, Ran et al. reported a curcumin-derivatized NIRF probe,[24] CRANAD-2, with difluoroboronate moiety. CRANAD-2 displayed high affinity to Aβ aggregates (K_d = 38.7 nM) and, upon binding to Aβ plaques, it displayed significant optical property changes. In vivo optical imaging studies indicated that CRANAD-2 exhibited a significantly higher relative signal in the brain of Tg2576 mice than that of control mice after intravenous injection; however, the clearance rate of CRANAD-2 from the brain is very slow, which is unfavorable for in vivo imaging. More recently, we reported a series of boron dipyrromethane (BODIPY) derivatives as NIRF probes for Aβ (BODIPY-7[25] and BAP-1[26]). Although they displayed high affinity to Aβ aggregates, their poor in vivo brain penetration and narrow Stokes shift lowered their practical application in vivo (Figure 2).

In an attempt to develop more practical NIRF imaging probes with a compact structure for in vivo detection of Aβ plaques, the donor−acceptor architecture bridged by a conjugated π-electron chain was selected as the backbone structure, and the design rationale for our NIRF probes (DANIRs) was based on three findings. First, the donor−acceptor substituted polymethine molecule is representative of an important class of organic nonlinear optical (NLO) chromophores.[27] Conjugation of double bonds could further induce a redshift in both absorption and emission spectra, and all fluorophores that have high absorption in the visible part of the spectrum possess several conjugated double bonds. By simple modification of the length of conjugated double bonds between the donor and acceptor groups, we could adjust the emission wavelength of DANIRs to the NIR range. Beyond the anticipated redshift, the binding affinity of the probes to Aβ plaques could be explored by this chemical modification. Second, the *N*,*N*′-dimethylamino group is well-known as the best absorption redshift pushing group for para-substituted aromatic rings,[28] and always acts as an important substituent for Aβ binding, as reported previously.[7,29] Thus, the *N*,*N*′-dimethylamino group was selected as the electron donor, and the dicyanomethylene group was selected as the electron acceptor. Finally, only one benzene ring was incorporated into the smart DANIR probes to reduce the lipophilicity and molecular weight of the probe significantly. In general, lipophilicity and molecular weight are considered to be important factors for BBB permeability. As a general rule, log *P* values between 2 and 3.5 are considered optimal, as higher log *P* values usually result in higher nonspecific binding and lead to a slow washout rate from the brain.[30] More importantly, the chemical structure of these DANIR probes is completely different from CR and ThT, which may provide useful information on the interaction between small molecules and Aβ fibers. Here we report the synthesis, characteristics, and biological evaluations of these donor−acceptor molecules as smart NIRF imaging probes for Aβ plaques in AD.

RESULTS AND DISCUSSION

The synthesis of DANIR probes is shown in Scheme 1. Aldehyde **1c** was prepared through the Wittig reaction from **1b**

Scheme 1. Synthetic Route for 2a−c[a]

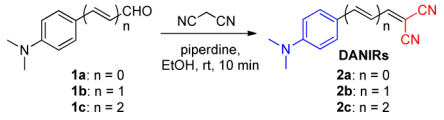

[a]NMR (^{1}H and ^{13}C) and HRMS data for **2a−c** are shown in Figures S1−3 in Supporting Information.

by following the reported procedure.[31] The final DANIR probes (**2a−c**) were prepared by condensation of the appropriate aldehydes with malononitrile in ethanol. The reaction could be completed within 10 min with high yield (69−92%), and the products (*E* isomer) were separated out as crystals without further purification. The straightforward synthesis of these probes is very favorable.

First, the fluorescent properties, including excitation and emission wavelengths of DANIRs in PBS (0.2 M, pH = 7.4), were evaluated. As anticipated, with the increase of the conjugated double bonds, the HOMO−LUMO energy gap becomes smaller, resulting in a significant redshift on the

dx.doi.org/10.1021/ja4052922 | J. Am. Chem. Soc. 2014, 136, 3388−3394

Table 1. Molecular Weight, Fluorescence Profile, Log *P* Values, and Fold Increase of the DANIR Probes upon Interaction with Aβ_{1-42} Aggregates

probe	MW	abs (nm)[a]	ε (M^{-1} cm^{-1})[a]	λ_{ex} (nm)[b]	λ_{em} (nm)[b]	Φ (%)[a,c]	fold increase	log P[d]
2a	197.24	433	76335	452	487	0	1.5	2.19
2b	223.27	489	128640	539	577	0.66	2.9	2.79
2c	249.31	519	50119	597	665	4.09	12.0	3.37

[a]Absorbance (abs) and molar extinction coefficient (ε) measured in CH_2Cl_2 (Figures S4−6 in Supporting Information). [b]Maximum excitation wavelength (λ_{ex}) and maximum emission wavelength (λ_{em}) measured in PBS. [c]Fluorescence quantum yield determined using a calibrated integrating sphere. [d]Log *P* values were calculated using online the ALOGPS 2.1 program.

emission wavelength. As shown in Table 1, the emission wavelengths for **2a**, **2b**, and **2c** were 487, 577, and 665 nm, respectively. The emission of **2c** was >650 nm in PBS, which falls in the best range for NIRF probes.

A useful NIRF Aβ-binding probe should significantly change its fluorescence properties upon binding to Aβ aggregates, while having weak interactions with serum albumin. Thus, we compared the fluorescent properties of all free probes in aqueous solution to their fluorescence properties in the presence of Aβ_{1-42} aggregates and bovine serum albumin (BSA). As shown in Figure 3, a significant fluorescence

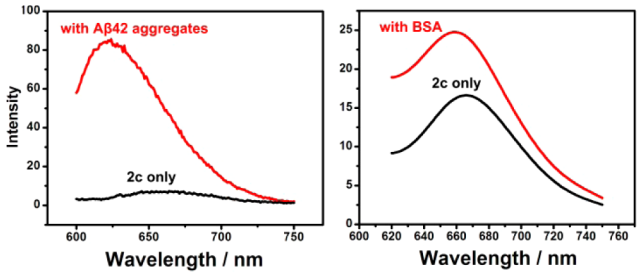

Figure 3. Fluorescence intensity of **2c** upon interaction with Aβ_{1-42} aggregates (left) and BSA (right).

intensity increase (12.0-fold) in the emission spectra of **2c** was observed upon association with Aβ_{1-42} aggregates. This intensity increase was also accompanied by a blueshift in the emission spectra of 40 nm. The blueshift of fluorescence emission maxima and the increase of fluorescence intensity could possibly show that **2c** binds to the hydrophobic pockets of aggregated amyloid fibrils and the mobility of **2c** is restricted. No significant change in fluorescence was observed during incubation with BSA, suggesting that there is little or no interaction between **2c** and BSA. In comparison with **2c**, probes **2a** and **2b** with shorter conjugated double bonds displayed weak interactions with both Aβ_{1-42} aggregates and BSA (Figures S7 and S8 in Supporting Information).

In vitro neuropathological fluorescent staining of Aβ plaques in slices of brain tissue from a double Tg (APPswe/PSEN1) mouse and AD patient was carried out to evaluate the affinity of these NIRF probes. As shown in Figure 4D and 4G, specific staining of plaques was observed in the brain slices of the Tg mouse with **2b** and **2c**. The presence and distribution of Aβ plaques was consistent with the results of staining adjacent slices using Thioflavin-S (Ths) (a common dye for staining Aβ plaques) (Figure 4E,H), while no such plaque staining was found when using **2a** (Figure 4A), which further confirmed that **2a** may have low affinity to Aβ plaques. Furthermore, intense labeling of plaques was observed in the brain slices of an AD patient (Figure 4C,F) with **2b** and **2c**. More interestingly, **2c** could also stain NFTs intensely in the entorhinal cortex region

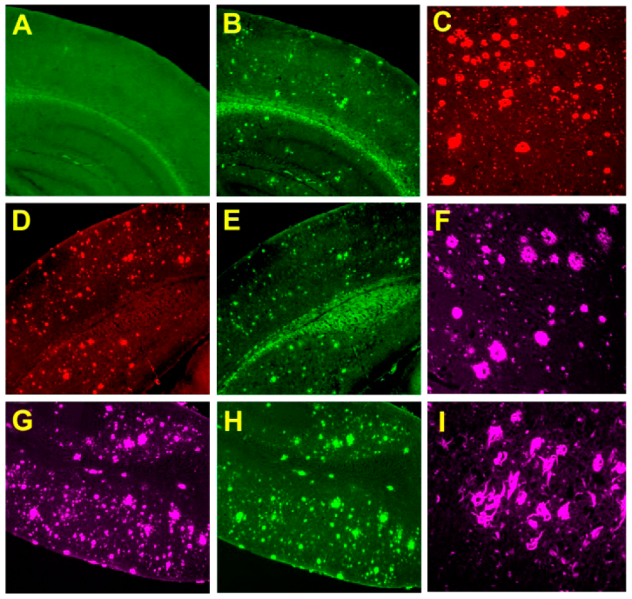

Figure 4. Neuropathological fluorescence staining of **2a−c** on brain slices from a double Tg mouse (C57BL6, APPsw/PSEN1, 12-month-old, male) (A, D, and G, cortex region, magnification: 5×) and AD patient (93-year-old, female) (C and F for **2b** and **2c** in the cortex region, I for **2c** in the entorhinal cortex, magnification: 10×). Adjacent slices from the Tg mouse were stained with ThS (B, E, and H, magnification: 5×). Green image for GFP filter set, red image for Tx-red filter set, and purple image for Cy5 filter set.

of the AD patient (Figure 4I), which indicates that **2c** has affinity to tangles.

To quantitatively evaluate the binding affinities of these probes to Aβ_{1-42} aggregates, an in vitro inhibition binding assay and saturation binding assay were carried out according to conventional methods. In the inhibition assay, these probes (**2a−c**) inhibited the binding of [^{125}I]IMPY in a dose-dependent manner (Figure S9A in Supporting Information). In the results shown in Table 2, probe **2a** displayed very poor affinity (K_i > 10000 nM), while **2b** and **2c** showed moderate to high affinity to Aβ_{1-42} aggregates as a result of the extension of conjugated double bonds (K_i = 518.8 and 36.9 nM, respectively), and these results were consistent with the

Table 2. Inhibition Constants (K_i, nM) and Dissociation Constant (K_d, nM) of 2a−c to Aβ_{1-42} Aggregates

probe	K_i (nM)[a]	K_d (nM)[a]
2a	>10000	1950 ± 189
2b	518.8 ± 29.3	35.8 ± 2.5
2c	36.9 ± 6.8	26.9 ± 3.0

[a]Measured in triplicate with results given as the mean ± SD.

dx.doi.org/10.1021/ja4052922 | J. Am. Chem. Soc. 2014, 136, 3388−3394

fluorescence intensity increase of these probes upon association with $A\beta_{1-42}$ aggregates and fluorescent staining experiments. In the saturation assay, the same phenomenon was also observed. The affinity gradually increased with the extension of conjugated double bonds with K_d values of 1950, 35.8, and 26.9 nM for **2a**, **2b**, and **2c**, respectively (Figure S9B–D in Supporting Information). The binding data of these probes indicated that the length of the conjugated double-bond bridge is crucial for Aβ binding. Several studies indicated that the conjugation and coplanar geometry of the ligand is very important for Aβ binding.[7] For this type of DANIR probe, the benzene plane and the dicyanomethylene plane are approximately coplanar in the extended conjugated π system.

More importantly, unlike other reported Aβ binding ligands with at least two aromatic rings, probe **2c** has only one benzene ring. It maintained high affinity to Aβ aggregates, which will provide new insight into the interactions between small molecules and Aβ fibers and will reduce the lipophilicity and molecular weight of the probe significantly. Probe **2c** with a molecular weight of 249 Da is likely to be among the simplest Aβ binding structures.

All synthesized compounds were found to have calculated log *P* values between 2.0 and 3.5 (Table 1), suggesting that they possess desirable properties for biocompatibility and can potentially cross the BBB efficiently. In addition, reasonable stability in blood and low cytotoxicity are two other important properties of a good NIR probe. In vitro stability studies indicated that **2c** has high in vitro stability in mouse serum, and more than 95% of the intact probe was identified after 60 min of incubation with mouse plasma at 37 °C (Figure S10 in Supporting Information). A cytotoxicity study of **2c** was performed by MTT assays with or without exposure to light using a human neuronal cell line (SH-SY5Y) at different concentrations. As shown in Figure 5, probe **2c** did not show

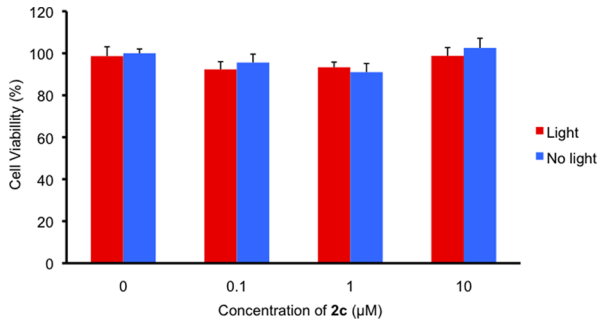

Figure 5. Cell viability after incubation of **2c** at different concentrations with a human neuronal cell line (SH-SY5Y) by MTT assay, at 37 °C for 24 h with or without exposure to light (each sample was tested using three replicates, and the results are reported as the mean ± standard deviation).

marked toxicity to this human neuronal cell line at 10 μM. Due to the high affinity of **2c** to Aβ aggregates, its emission falling in the range for NIR, high stability in mouse serum, and low cytotoxicity to human neuronal cells, probe **2c** was selected for further in vivo evaluations.

Although the unique advantage of optical imaging is the possibility of producing substantial differences in the photophysical/optical properties between the bound and unbound forms of the probe, the fast washout of the unbound probe in the target organs will provide an enhanced signal-to-noise ratio. In vivo NIR imaging of normal nude mice (SS111-BALB/ca, 6-week-old, female) was carried out to evaluate the brain kinetics, absorption, distribution, and excretion of **2c** in normal mice (injected dose: 0.4 mg/kg, 20% DMSO, 80% propylene glycol, 50 μL). As shown in Figure S11 in Supporting Information, **2c** could penetrate the BBB efficiently and was quickly washed out of the normal brain. After 60 min postinjection, almost all the probes had been eliminated from the brain, which are highly desirable properties for Aβ NIRF imaging probes. In addition, **2c** was excreted by the intestines, where fluorescence signals were mainly accumulated (Figure S12 in Supporting Information). In addition, a direct comparison of the brain kinetics between **2c** and the BODIPY-based derivative BAP-1 was performed by ex vivo imaging of the brains of normal mice, as shown in Figure S13 in Supporting Information, and **2c** ($brain_{2\ min}/brain_{30\ min}$ ratio: 5.66) cleared much faster than BAP-1 ($brain_{2\ min}/brain_{30\ min}$ ratio: 1.82).

Finally, 22-month-old female double Tg mice (C57BL6, APPsw/PSEN1) and age-matched wild-type mice (C57BL6) were used to assess the potential of **2c** for specific amyloid plaque imaging in vivo using NIRF imaging. As shown in Figure 6, the fluorescence signal diminished considerably more slowly

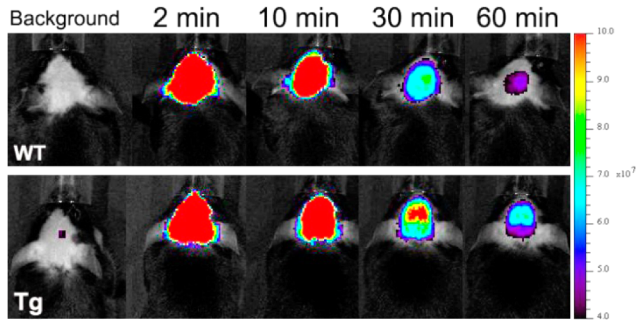

Figure 6. NIRF images of Tg mice and control mice at different time points before and after iv injection of **2c** (0.4 mg/kg).

in the 22-month-old Tg mice than in the wild-type control. Fluorescence intensities in the brain regions of the Tg mice were higher than in the control mice 30 min after iv injection of **2c**. More imaging details are shown in Figure S14 in Supporting Information. Brain kinetic curves were obtained by semi-quantitative analysis of the images, which was performed by selecting a region of interest (ROI) in the brain (Figure 7). There was a significant difference in the clearance profile after the administration of **2c** between Tg and wild-type control

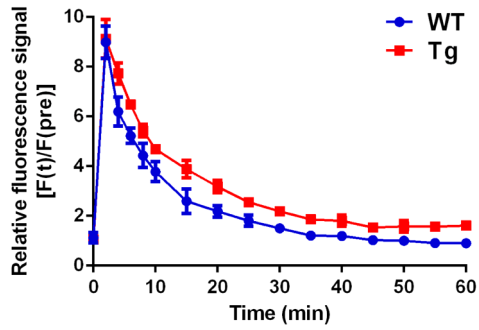

Figure 7. The relative fluorescence signal $[F(t)/F(\text{pre})]$ in the brain regions of Tg mice and control mice after iv injection of **2c** (n = 3, 0.4 mg/kg). The $[F(t)/F(\text{pre})]$ of Tg mice was significantly higher than that of the control mice ($p < 0.05$).

dx.doi.org/10.1021/ja4052922 | J. Am. Chem. Soc. 2014, 136, 3388–3394

mice ($p < 0.05$), and the higher fluorescence signal in the brain of Tg mouse may have resulted from the binding of **2c** with Aβ plaques.

To further confirm the binding of **2c** to Aβ plaques in vivo, ex vivo histology was carried out in Tg mice and wild-type control mice. Thirty minutes after iv injection of **2c**, a higher number of Aβ plaques were observed in the brain slices from Tg mice (Figure 8A); however, no plaques were found in the age-matched control mice (Figure 8C). In addition, the Aβ plaques were further confirmed by staining the same section with ThS (Figure 8B,D). These results further confirmed our in vivo NIRF imaging data that **2c** could penetrate the BBB and label Aβ plaques specifically in vivo.

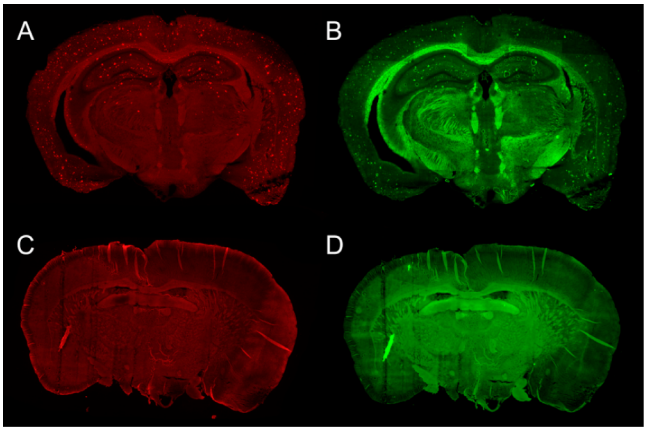

Figure 8. Ex vivo fluorescence observation (Cy5 filter set) of brain slices from a Tg mouse (A) and wild-type control mouse (C) after injection of **2c**. The Aβ plaques were further confirmed by staining the same sections with ThS (GFP filter set, B, D).

CONCLUSION

We successfully designed and synthesized a series of novel smart NIRF probes with donor−acceptor architecture for in vivo detection of Aβ plaques. One probe, **2c**, with a longer conjugated double bond system, displayed maximum emission in PBS (665 nm). Upon binding to Aβ_{1-42} aggregates, **2c** displayed a significant fluorescence intensity increase and a blueshift (625 nm) in the emission spectra, which is very close to the best range for NIR imaging. In binding experiments in vitro, **2c** showed high affinity for Aβ_{1-42} aggregates (K_i = 37 nM, K_d = 27 nM). On NIRF imaging, there was a significant difference in the clearance profile after the administration of **2c** between Tg and wild-type control mice, and the specific binding of **2c** to Aβ plaques was further confirmed by ex vivo histology. In summary, this smart probe meets most of the requirements for a NIRF contrast agent for the detection of Aβ plaques both in vitro and in vivo.

EXPERIMENTAL SECTION

General Information. All reagents used in the synthesis were commercial products and were used without further purification unless otherwise indicated. The ^{1}H NMR spectra were obtained at 400 MHz on JEOL JNM-AL400 NMR spectrometers in $CDCl_3$ solutions at room temperature (rt) with tetramethylsilane (TMS) as an internal standard. Chemical shifts were reported as δ values with respect to residual solvents. The ^{13}C NMR spectra were obtained at 100 MHz on a Bruker spectrometer in $CDCl_3$ at rt. Multiplicity is defined by s (singlet), d (doublet), t (triplet), m (multiplet). Reactions were monitored by TLC (TLC Silica gel 60 F_{254}, Merck). HPLC was performed with a Shimadzu system (a LC-20AT pump with a SPD-20A UV detector, λ = 254 nm) using a Venusil MP C18 column (Agela Technologies, 10 μm, 4.6 mm × 250 mm) eluted with a binary gradient system at a 1.0 mL/min flow rate. Mobile phase A was water while mobile phase B was acetonitrile. Fluorescence studies were carried out with an RF-5301PC fluorescence spectrophotometer (Shimadzu, Kyoto, Japan). Quantum yields of all samples were recorded on a Fluoromax 4 with a calibrated intergrating sphere system (Horiba Jobin Yvon, France). The absorbance spectrum of the solution was measured using a UV-2450 spectrophotometer (Shimadzu, Kyoto, Japan). Fluorescent observation was performed using a BZ-9000 (Keyence, Itasca, IL) and an Axio Oberver Z1 (Zeiss, Germany) equipped with GFP and Cy5 filter sets. The purity of the synthesized key compounds was determined using analytical HPLC and was found to be more than 95%. Normal nude mice (SS111-BALB/ca, 6-week-old, male) were used for in vivo imaging experiments. Double transgenic mice (C57BL6, APPsw/PSEN1, 22-month-old, female), used as an Alzheimer's model, were purchased from the Institute of Laboratory Animal Sciences, Chinese Academy of Medical Sciences. All protocols requiring the use of mice were approved by the animal care committee of Kyoto University and Beijing Normal University. Postmortem brain tissues from an autopsy confirmed case of AD (93-year-old, female) were obtained from the Graduate School of Medicine, Kyoto University. Experiments were performed according to the regulations of the ethics committee of Kyoto University.

Chemistry. *2-(4-(Dimethylamino)benzylidene)malononitrile (**2a**).* To a solution of 300 mg of 4-(dimethylamino)benzaldehyde (2 mmol) and 132 mg of malononitrile (2 mmol) in ethanol was added 200 μL of piperdine, the reaction mixture was stirred at rt for 10 min, a yellow crystal was formed, and the crystal was filtered and washed by hexane, yield: 92.0%. ^{1}H NMR (400 MHz, $CDCl_3$) δ 7.82 (d, J = 9.0 Hz, 2H), 7.47 (s, 1H), 6.69 (d, J = 9.1 Hz, 2H), 3.14 (s, 6H). ^{13}C NMR (125 MHz, $CDCl_3$): δ 157.98, 154.19, 133.73, 119.19, 115.96, 114.89, 111.54, 71.65, 40.02. HRMS(EI): m/z calcd for $C_{12}H_{11}N_3$ 197.0953; found 197.0948. Anal. Calcd: C 73.07, H 5.62, N 21.30; Found: C 73.02, H 5.68, N 21.25.

*(E)-2-(3-(4-(Dimethylamino)phenyl)allylidene)malononitrile (**2b**).* The same reaction as described above for preparing **2a** was employed, and a dark red crystal of **2b** was obtained (90.0% yield). ^{1}H NMR (400 MHz, $CDCl_3$) δ 7.48 (m, 3H), 7.17 (d, J = 14.8 Hz, 1H), 7.02 (dd, J = 14.8, 11.7 Hz, 1H), 6.68 (d, J = 9.0 Hz, 2H), 3.10 (s, 6H). ^{13}C NMR (125 MHz, $CDCl_3$): δ 160.44, 153.02, 151.53, 131.57, 121.76, 117.16, 114.98, 113.07, 111.89, 40.04. HRMS(EI): m/z calcd for $C_{14}H_{13}N_3$ 223.1109; found 223.1115. Anal. Calcd: C 75.31, H 5.87, N 18.82; Found: C 75.08, H 5.94, N 18.76.

*2-((2E,4E)-5-(4-(Dimethylamino)phenyl)penta-2,4-dien-1-ylidene)malononitrile (**2c**).* The same reaction as described above for preparing **2a** was employed, and a dark purple crystal of **2c** was obtained (69.0% yield). ^{1}H NMR (400 MHz, $CDCl_3$) δ 7.42 (m, 3H), 7.06 (dd, J = 14.4, 11.2 Hz, 1H), 6.97 (d, J = 14.8 Hz, 1H), 6.80 (dd, J = 15.2, 11.2 Hz, 1H), 6.72 (d, J = 14.6 Hz, 1H), 6.68 (d, J = 9.2 Hz, 2H), 3.06 (s, 6H). ^{13}C NMR (125 MHz, $CDCl_3$): δ 159.52, 152.10, 151.88, 146.40, 130.00, 123.36, 123.09, 121.99, 114.73, 112.72, 111.94, 40.06. HRMS(EI): m/z calcd for $C_{16}H_{15}N_3$ 249.1266; found 249.1259 ($M + H^+$). Anal. Calcd: C 77.08, H 6.06, N 16.85; Found: C 76.95, H 6.04, N 16.73.

Fluorescence Studies upon Binding to Aβ_{1-42} Aggregates and BSA. A solution of 100 μL of aggregated Aβ_{1-42} fibrils (20 μg in the final assay mixture) or BSA (20 μg in the final assay mixture) was added to the mixture containing NIR probes (100 μL, 1 μM in EtOH) and 800 μL of PBS (0.2 M, pH = 7.4) in a final volume of 1 mL. The mixture was incubated for 30 min at rt, the solution was transferred to a quartz sampling cell, and the fluorescent parameters (fluorescence excitation/emission wavelength and intensity) were measured by a RF-5301PC fluorescence spectrophotometer (Shimadzu).

In Vitro Fluorescent Staining of Aβ Plaques in Transgenic Mouse Brain Sections and Human Brain Materials. Paraffin-embedded brain tissue from double transgenic mice (C57BL6, APPsw/PSEN1, 12 months old, male) and an AD human (93-year-

dx.doi.org/10.1021/ja4052922 | J. Am. Chem. Soc. 2014, 136, 3388−3394

old, female) were used for in vitro fluorescent staining. The brain sections were deparaffinized with 2 × 20 min washes in xylene, 2 × 5 min washes in 100% ethanol, 5 min washes in 90% ethanol/H_2O, 5 min washes in 80% ethanol/H_2O, a 5 min wash in 60% ethanol/H_2O, and running tap water for 10 min and then incubated in PBS (0.2 M, pH = 7.4) for 30 min. Next, they were incubated with a 10% ethanol solution (1 μM) of NIR probes (**2a**−**c**) for 5 min. The location of plaques was confirmed by staining adjacent sections with ThS (0.125%). Finally, the sections were washed with 40% ethanol and PBS (0.2 M, pH = 7.4) for 10 min. Fluorescent observation was performed using a BZ-9000 (Keyence) equipped with GFP and Cy5 filter sets.

In Vitro Inhibition Binding Studies Using Aβ_{1-42} Aggregates. The trifluoroacetic acid salt forms of peptides Aβ_{1-42} were purchased from Osaka Peptide Institute (Osaka, Japan). Aggregation of peptides was carried out by gently dissolving the peptide [0.25 mg/mL for Aβ_{1-42}] in a buffer solution (pH = 7.4) containing 10 mM potassium dihydrogen phosphate and 1 mM EDTA. The solutions were incubated at 37 °C for 42 h with gentle and constant shaking. Inhibition experiments were carried out in 12 × 75 mm borosilicate glass tubes according to the procedures described previously with some modifications. Briefly, 100 μL of aggregated Aβ fibrils (60 nM in the final assay mixture) was added to a mixture containing 100 μL of radioligands ([^{125}I]IMPY) at an appropriate concentration, 10 μL of inhibitors (10^{-5} to 10^{-10} M in ethanol), and 790 μL of PBS (0.2 M, pH = 7.4) in a final volume of 1 mL. Nonspecific binding was defined in the presence of 1 μM IMPY. The mixture was incubated for 2 h at 37 °C with constant shaking, and then the bound and free radioactive fractions were separated by vacuum filtration through borosilicate glass fiber filters (Whatman GF/B) using a M-24 cell harvester (Brandel, Gaithersburg, MD). The radioactivity from filters containing the bound ^{125}I ligand was measured in a γ-counter (Wallac/Wizard 1470, PerkinElmer, Waltham, MA) with 70% efficiency. Under the assay conditions, the specifically bound fraction accounted for about 10% of total radioactivity. The half maximal inhibitory concentration (IC_{50}) was determined using GraphPad Prism 4.0, and the inhibition constant (K_i) was calculated using the Cheng−Prusoff equation:[32] $K_i = IC_{50}/(1 + [L]/K_d)$.

In Vitro Saturation Binding Studies Using Aβ_{1-42} Aggregates. A solution of 100 μL of aggregated Aβ_{1-42} fibrils (10 μg in the final assay mixture) was added to the mixture containing 100 μL of NIR probes ($10^{-5.5}$ to 10^{-10} nM in EtOH) and 800 μL of PBS (0.2 M, pH = 7.4) in a final volume of 1 mL. Nonspecific binding was defined without NIR probes. The mixture was incubated for 30 min at rt, the solution was transferred to a black 96-well plate, and the fluorescent intensity was measured by an Infinite F200 Multifunction microplate reader (Tecan, Austria). The results of saturation experiments were calculated using GraphPad Prism 4.0.

In Vitro Stability Studies of 2c in Mouse Serum. The in vitro stability of **2c** in mouse serum was determined by incubating **2c** (50 μL, 10% ethanol solution, 10 μM) with 300 μL of mouse serum at 37 °C for 30 and 60 min. Proteins were precipitated by adding 500 μL of acetonitrile after centrifugation at 5000 rpm for 5 min at 4 °C. The supernatant was collected. Approximately 0.1 mL of the supernatant solution was analyzed using HPLC (UV detector, λ = 254 nm).

Cytotoxicity Studies. This assay measures the viability of living cells (SH-SY5Y, human neuronal cell line) via the cleavage of MTT [3-(4,5-dimethylthiazol-2-yl)-2,5-diphenyltetrazolium bromide] to purple formazan crystals by the cell mitochondrial dehydrogenases. SH-SY5Y cells were seeded into a 24-well plate and incubated at 37 °C in a humidified atmosphere with 5% CO_2. Then the cells were treated with at different concentrations of **2c** (0, 0.1, 1, and 10 μM) for 1 h incubation and then exposed to a laser of an Ivis Spectrum imaging system (excitation: 605 nm, exposure time: 1s) or not. After further incubation for 24 h, MTT solution (3 mg/mL) was added, and the cells were incubated for another 20 min. The absorbance of each well was measured at 570 nm (Infinite M200PRO, Tecan).

In Vivo Near-Infrared Imaging of 2c on Nude Mouse. In vivo NIR imaging was performed on a Xenogen IVIS 200 Imaging station (Xenogen, Alameda, CA). Images were acquired and analyzed using Living Image software. A normal nude mouse was iv injected with **2c** (0.4 mg/kg, 20% DMSO, 80% propylene glycol, 50 μL). Fluorescence signals were recorded at different time points after iv injection of **2c**. For the measurement, a filter set (ex. at 605 nm and em. at 680 nm) was used, and optical images were acquired using an exposure time of 1 s. During the imaging process, the mice were kept on the imaging stage under anesthesia with 2.5% isoflurane gas in an oxygen flow (1.5 L/min).

In Vivo Near-Infrared Imaging of 2c on Tg Mouse and Wild-Type Mouse. Double transgenic mouse (n = 3, C57BL6, APPsw/PSEN1, 22-month-old, female) and an age-matched control mouse (n = 3, C57BL6, 22-months-old, female) were shaved before background imaging and were iv injected with **2c** (0.4 mg/kg, 20% DMSO, 80% propylene glycol, 50 μL). Fluorescence signals from the brain were recorded at different time points after iv injection of **2c**. For the measurement, a filter set (ex. at 605 nm and em. at 680 nm) was used, and optical images were acquired using an exposure time of 1 s. During the imaging process, the mice were kept on the imaging stage under anesthesia with 2.5% isoflurane gas in an oxygen flow (1.5 L/min). Imaging data was analyzed by Living Image software, and an ROI was drawn around the brain region. Intensity of brain fluorescence was calculated from the photon counts. The data were analyzed by normalizing the fluorescence intensity to the background fluorescence of each mouse [i.e., $F(t)/F(\mathrm{pre})$], where $F(t)$ is the fluorescence intensity of the time point of interest and $F(\mathrm{pre})$ is the background fluorescence signal. P values were calculated by Student's t test.

Ex Vivo Fluorescent Staining of 2c to Aβ Plaques in Transgenic Mouse Brain. One week after in vivo imaging, the double transgenic mouse (C57BL6, APPsw/PSEN1, 22-month-old, female) and an age-matched control mouse (C57BL6, 22-month-old, female) were iv injected with **2c** (0.4 mg/kg, 20% DMSO, 80% propylene glycol, 50 μL) and sacrificed at 30 min after injection. The brains were excised, embedded in optimum cutting temperature compound (OCT), and frozen in powdered dry ice immediately. Frozen sections of 20 μm were cut, and fluorescent observation was performed by Axio Oberver Z1 (Zeiss) equipped with a Cy5 filter set. In addition, the Aβ plaques were further confirmed by the staining of the same section with ThS (0.125%) using a GFP filter set.

■ ASSOCIATED CONTENT

Ⓢ Supporting Information

General materials and methods, including Aβ_{1-42} aggregates and BSA interactions, in vitro and in vivo biological evaluations of **2a**−**c**, and nine figures, as described in the text. This material is available free of charge via the Internet at http://pubs.acs.org.

■ AUTHOR INFORMATION

Corresponding Author

ono@pharm.kyoto-u.ac.jp

Notes

The authors declare no competing financial interests.

■ ACKNOWLEDGMENTS

This research was funded by the Japan Society for the Promotion of Science (JSPS) through the "Funding Program for Next Generation World-Leading Researchers (NEXT Program)," initiated by the Council for Science and Technology Policy (CSTP), the National Natural Science Foundation of China (no. 21201019), and the Research Fund for the Doctoral Program of Higher Education of China (no. 20120003120013). This study was also supported by the China Scholarship Council (CSC). The authors give special thanks to Dr. Liandi Lei (Laboratory of Molecular Imaging, Health Science Analysis Center, Peking University) for assistance with the in vivo NIRF imaging, Dr. Cuihong Li (College of Chemistry, Beijing Normal University) for assistance with the

measurement of fluorescence quantum yield, Dr. Hiro Amano (Department of Patho-Functional Bioanalysis, Graduate School of Pharmaceutical Sciences, Kyoto University) for assistance with the cytotoxicity tests, and Dr. Masafumi Ihara (Department of Neurology, Graduate School of Medicine, Kyoto University) for providing AD brain sections.

REFERENCES

(1) Selkoe, D. J. *JAMA, J. Am. Med. Assoc.* **2000**, *283*, 1615−1617.
(2) Selkoe, D. J. *Physiol. Rev.* **2001**, *81*, 741−766.
(3) Hardy, J. A.; Higgins, G. A. *Science* **1992**, *256*, 184−185.
(4) Hardy, J. A.; Selkoe, D. J. *Science* **2002**, *297*, 353−356.
(5) Hardy, J.*Neurobiol. Aging* **1999**, *20*, 85, discussion 87.
(6) Kung, H. F. *ACS Med. Chem. Lett.* **2012**, *3*, 265−267.
(7) Cai, L.; Innis, R. B.; Pike, V. W. *Curr. Med. Chem.* **2007**, *14*, 19−52.
(8) Quigley, H.; Colloby, S. J.; O'Brien, J. T. *Int. J. Geriatr. Psychiatry* **2011**, *26*, 991−999.
(9) Rowe, C. C.; Villemagne, V. L. *J. Nucl. Med.* **2011**, *52*, 1733−1740.
(10) Mathis, C. A.; Mason, N. S.; Lopresti, B. J.; Klunk, W. E. *Semin. Nucl. Med.* **2012**, *42*, 423−432.
(11) Mathis, C. A.; Wang, Y.; Holt, D. P.; Huang, G. F.; Debnath, M. L.; Klunk, W. E. *J. Med. Chem.* **2003**, *46*, 2740−2754.
(12) Klunk, W. E.; Engler, H.; Nordberg, A.; Wang, Y.; Blomqvist, G.; Holt, D. P.; Bergstrom, M.; Savitcheva, I.; Huang, G. F.; Estrada, S.; Ausen, B.; Debnath, M. L.; Barletta, J.; Price, J. C.; Sandell, J.; Lopresti, B. J.; Wall, A.; Koivisto, P.; Antoni, G.; Mathis, C. A.; Langstrom, B. *Ann. Neurol.* **2004**, *55*, 306−319.
(13) Kadir, A.; Marutle, A.; Gonzalez, D.; Scholl, M.; Almkvist, O.; Mousavi, M.; Mustafiz, T.; Darreh-Shori, T.; Nennesmo, I.; Nordberg, A. *Brain* **2011**, *134*, 301−317.
(14) Choi, S. R.; Golding, G.; Zhuang, Z.; Zhang, W.; Lim, N.; Hefti, F.; Benedum, T. E.; Kilbourn, M. R.; Skovronsky, D.; Kung, H. F. *J. Nucl. Med.* **2009**, *50*, 1887−1894.
(15) Wong, D. F.; Rosenberg, P. B.; Zhou, Y.; Kumar, A.; Raymont, V.; Ravert, H. T.; Dannals, R. F.; Nandi, A.; Brasic, J. R.; Ye, W.; Hilton, J.; Lyketsos, C.; Kung, H. F.; Joshi, A. D.; Skovronsky, D. M.; Pontecorvo, M. J. *J. Nucl. Med.* **2010**, *51*, 913−920.
(16) Lin, K. J.; Hsu, W. C.; Hsiao, I. T.; Wey, S. P.; Jin, L. W.; Skovronsky, D.; Wai, Y. Y.; Chang, H. P.; Lo, C. W.; Yao, C. H.; Yen, T. C.; Kung, M. P. *Nucl. Med. Biol.* **2010**, *37*, 497−508.
(17) Camus, V.; Payoux, P.; Barre, L.; Desgranges, B.; Voisin, T.; Tauber, C.; La Joie, R.; Tafani, M.; Hommet, C.; Chetelat, G.; Mondon, K.; de La Sayette, V.; Cottier, J. P.; Beaufils, E.; Ribeiro, M. J.; Gissot, V.; Vierron, E.; Vercouillie, J.; Vellas, B.; Eustache, F.; Guilloteau, D. *Eur. J. Nucl. Med. Mol. Imaging* **2012**, *39*, 621−631.
(18) Ntziachristos, V.; Bremer, C.; Weissleder, R. *Eur. Radiol.* **2003**, *13*, 195−208.
(19) Ntziachristos, V. *Annu. Rev. Biomed. Eng.* **2006**, *8*, 1−33.
(20) Frangioni, J. V. *Curr. Opin. Chem. Biol.* **2003**, *7*, 626−634.
(21) Licha, K.; Olbrich, C. *Adv. Drug Delivery Rev.* **2005**, *57*, 1087−1108.
(22) Hintersteiner, M.; Enz, A.; Frey, P.; Jaton, A. L.; Kinzy, W.; Kneuer, R.; Neumann, U.; Rudin, M.; Staufenbiel, M.; Stoeckli, M.; Wiederhold, K. H.; Gremlich, H. U. *Nat. Biotechnol.* **2005**, *23*, 577−583.
(23) Nesterov, E. E.; Skoch, J.; Hyman, B. T.; Klunk, W. E.; Bacskai, B. J.; Swager, T. M. *Angew. Chem., Int. Ed. Engl.* **2005**, *44*, 5452−5456.
(24) Ran, C.; Xu, X.; Raymond, S. B.; Ferrara, B. J.; Neal, K.; Bacskai, B. J.; Medarova, Z.; Moore, A. *J. Am. Chem. Soc.* **2009**, *131*, 15257−15261.
(25) Ono, M.; Ishikawa, M.; Kimura, H.; Hayashi, S.; Matsumura, K.; Watanabe, H.; Shimizu, Y.; Cheng, Y.; Cui, M.; Kawashima, H.; Saji, H. *Bioorg. Med. Chem. Lett.* **2010**, *20*, 3885−3888.
(26) Ono, M.; Watanabe, H.; Kimura, H.; Saji, H. *ACS Chem. Neurosci.* **2012**, *3*, 319−324.
(27) Meyers, F.; Marder, S. R.; Pierce, B. M.; Bredas, J. L. *J. Am. Chem. Soc.* **1994**, *116*, 10703−10714.
(28) *Organic Structure Analysis*; Crews, P.; Rodriguez, J.; Jaspars, M., Eds.; Oxford University Press: New York, 1998.
(29) Cui, M.; Ono, M.; Kimura, H.; Kawashima, H.; Liu, B. L.; Saji, H. *Nucl. Med. Biol.* **2011**, *38*, 313−320.
(30) Ametamey, S. M.; Honer, M.; Schubiger, P. A. *Chem. Rev.* **2008**, *108*, 1501−1516.
(31) Plażuk, D.; Janowska, I.; Kłys, A.; Hameed, A.; Zakrzewski, J. *Synth. Commun.* **2003**, *33*, 381−385.
(32) Cheng, Y.; Prusoff, W. H. *Biochem. Pharmacol.* **1973**, *22*, 3099−3108.